Molecular Catalysis 590 (2026) 115621

Contents lists available at ScienceDirect

Molecular Catalysis

journal homepage: www.journals.elsevier.com/molecular-catalysis

Coupling reactions of ethanol and an ethanol/acetaldehyde mixture over Mo/MgO-SiO_2 catalysts

Gyula Novodárszki [a,b], Adél Pakuts [a], Blanka Szabó [c], Hanna E. Solt [a], Anna Vikár [a], Ferenc Lónyi [a], Yuting Shi [a,d], Amosi Makoye [a,e], Róbert Barthos [a,*]

[a] HUN-REN Research Centre for Natural Sciences, Magyar Tudósok Krt. 2, H-1117, Budapest, Hungary
[b] Instiute of Chemistry, ELTE Eötvös Loránd University, Pázmány Péter sétány 1/A, 1117, Budapest, Hungary
[c] Centrale Méditerranée, L'Institut des Sciences Moléculaires de Marseille, St Jérôme Aix Marseille Université 52 Avenue Escadrille Normandie Niemen 13013 Marseille, France
[d] Doctoral School of Environmental Science, ELTE Eötvös Loránd University, Pázmány Péter sétány 1/A, 1117, Budapest, Hungary
[e] Hevesy György Doctoral School of Chemistry, ELTE Eötvös Loránd University, Pázmány Péter sétány 1/A, 1117, Budapest, Hungary

ARTICLE INFO

Keywords:
Ethanol
Acetaldehyde
Molybdenum oxide
MgO-SiO_2 catalysts
Butadiene

ABSTRACT

Acetaldehyde has been identified as a key intermediate in the catalytic conversion of ethanol into butadiene or butanol. A variety of methodologies have been implemented to enhance the yield, including the promotion of in situ catalytic generation of acetaldehyde and the direct addition of acetaldehyde to the ethanol reactant. In the present study, molybdenum-promoted, partially silica-coated magnesium oxide catalysts (Mo/MgO-SiO_2) were prepared and utilized. The initiation of an intermolecular redox reaction by molybdenum led to the conversion of ethanol to acetaldehyde and ethane. However, the Mo-promoted catalyst exhibited lower basicity and, consequently, reduced activity in aldol coupling when compared to the supporting oxide. The conversion of ethanol and the yield of C_4 were found to be higher in the presence of the Mo-promoted catalysts in comparison to the MgO-SiO_2 support, yet butadiene selectivity was observed to be lower. The conversion of an ethanol/acetaldehyde mixture resulted in a substantial butadiene yield, accompanied by notable crotonaldehyde and crotyl alcohol yields. It is noteworthy that the latter two products were not obtained from pure ethanol. At elevated space velocities, two additional condensation products, ethyl vinyl ether and ethyl acetate, were obtained from the mixture. This suggests that the coupled products are formed not only by the condensation of two acetaldehyde molecules, but also by other coupling pathways occurring between intermediate products that are adsorbed on the catalyst surface.

1. Introduction

The push for carbon neutrality is prompting the chemical industry to increasingly use more renewable carbon sources. Although four-carbon compounds can be efficiently prepared by coupling bioethanol using heterogeneous catalytic processes, 1,3-butadiene and butanol are still mainly produced from fossil carbon sources [1,2]. The most commonly used catalysts for the ethanol-to-butadiene (ETBD) reaction are MgO-SiO_2 [3–5], ZrO_2-SiO_2 [6–8] and their metal or metal oxide doped derivatives [9–15]. Catalysts based on MgO-Al_2O_3 [16–18] and hydroxyapatite [19,20] are mainly used for the synthesis of butanol (ETBL).

A number of studies suggested that the ethanol coupling proceeds by aldol mechanism [5,21–23]. Accordingly, the reaction is initiated by catalytic formation of acetaldehyde from ethanol. The aldol condensation of acetaldehyde over a catalyst gives crotonaldehyde. In consecutive reaction step crotonaldehyde can get transfer hydrogenated by ethanol [Meerwein–Ponndorf–Verley (MPV) reaction], giving acetaldehyde and crotyl alcohol. The dehydration of crotyl alcohol can result in 1,3-butadiene, whereas its double bond hydrogenation can give 1-butanol. The selectivity depends on the relative rate of mentioned activities whereas the rate of the reaction and the conversion is determined by the rate-controlling step of the process. It follows from the aldol mechanism that the moderate dehydrogenation/hydrogen transfer activity of the mixed oxide catalysts might control the rate of acetaldehyde and, thereby, the rate of the C_4 formation. Therefore, it is

* Corresponding author.
E-mail address: barthos.robert@ttk.hu (R. Barthos).

https://doi.org/10.1016/j.mcat.2025.115621
Received 7 October 2025; Received in revised form 10 November 2025; Accepted 21 November 2025
Available online 1 December 2025

reasonable to co-feed acetaldehyde and ethanol or to use a mixed oxide catalyst having higher dehydrogenation and hydrogen transfer activity. A transition metal component can enhance latter activities, however, it modifies also the activities in the condensation coupling and dehydration reactions initiated by basic and acidic surface sites.

Some results have called into question the central role of the acetaldehyde intermediate in the reaction. It has been proposed that butanol could be produced in one step via the direct condensation of two ethanol molecules [17,24–27]. Another alternative to the aldol mechanism involves forming the crotyl alcohol intermediate through the coupling of ethanol and acetaldehyde. This latter process is also known as the semi-direct mechanism of 1,3 butadiene or butanol formation. Some authors have concluded that any of these coupling mechanisms can dominate under certain reaction conditions [28].

The ETBD reaction can be performed using either the one-step Lebedev method with pure ethanol or the two-step Ostromislensky method with a mixture of ethanol and acetaldehyde. The acetaldehyde that is used as a reactant must be synthesized separately. In the two-step process the acetaldehyde is available in the reactor regardless of the dehydrogenating and MPV activity of the catalyst. Although it could be beneficial, the two-step procedure is not used in the ETBOL process.

Clearly, both aldol condensation and the MPV reaction must occur to produce crotyl alcohol, a common intermediate in the formation of 1,3-butadiene and butanol. Thus, maximizing the rate of crotyl alcohol formation requires an optimal aldehyde/ethanol ratio. Kinetic studies and experiments with acetaldehyde containing isotopically labeled carbon suggest that aldol condensation occurs via the Redel-Eley mechanism [29]. Li et al. [7] substantiated a bimolecular synergetic adsorption mechanism. In brief, the active catalyst surface is covered by enolate and ethoxy species. The gas phase above the catalyst contains acetaldehyde that was either added to and/or generated from ethanol. Aldol condensation has been shown to occur between the gas-phase acetaldehyde and the surface-bound acetaldehyde enolate. The enol form of the obtained aldol dimer (i.e., 3-hydroxybut-1-en-1-ol) is readily dehydrated to crotyl aldehyde enolate. In the MPV reaction, ethanol reacts with surface enolate species, releasing crotyl alcohol and acetaldehyde and regenerating active ethoxy species.

Transition metal oxides have been extensively studied as catalysts or components of catalysts in the ETBD and ETBL reactions. However, little attention has been given to molybdena [18,30–32]. Under comparable reaction conditions, the MgO-Al_2O_3 mixed oxide catalyst containing the molybdenum component produced higher yields of butanol and 1, 3-butadiene than the molybdenum-free mixed oxide [18]. However, the activity loss of the catalyst was significant. In general, the MgO-Al_2O_3 mixed oxide supporting a transition metal oxide had enhanced dehydrogenation activity relative to the support, but significantly reduced basicity and, therefore, ethanol coupling activity [30]. Only minor amount of C4 product was obtained using molydena-silica catalysts, most likely because their acid-base properties did not favor the ethanol coupling reactions [31,32]. With the Mo(VI) catalyst, ethylene and acetaldehyde were the main products with selectivites of 28 and 66 %, respectively. The Mo(IV)-containing catalyst had a lower initial activity, yielding acetaldehyde and ethane with nearly equal selectivity of about 47 % [32]. It has been proposed that ethane and acetaldehyde form simultaneously via an intermolecular hydrogen transfer reaction between two adjacent ethanol molecules adsorbed on Mo^{4+}–O^{2-} Lewis acid- Lewis base pair sites. The Mo(IV) can be obtained from Mo(VI) through slow reduction by the ethanol feed. One aspect of the present study is to learn about the ethanol coupling activity of the strong base MgO-SiO_2-supported molybdena catalysts.

The two most common methods for synthesizing MgO-SiO_2 mixed oxide catalysts are co-precipitation [33,34] and wet kneading [35–38]. Co-precipitation results in a homogeneous mixed oxide, whereas wet kneading results in a structure, consisting of contacting micro-size islands of the two oxides [39]. Mg-O-Si bonds are formed only at the contact surfaces [5]. The MgO phase is basic, whereas the Mg-O-Si bonds formed at the phase boundaries have acidic properties. Mainly the basic sites are responsible for the aldol coupling activity [40]. The number and strength of the acid sites ensure the appropriate dehydrating activity [33,41]. Recently, Chung et al. [38] thoroughly investigated the wet-kneading process and discovered that adjusting the pH of the mother liquor properly can result in MgO-coated SiO_2 or SiO_2-coated MgO structures. The latter preparations were found to be more efficient catalysts in the ETBD process. Namely, when wet kneading is performed at a pH of 11.4, a Si-OH-Mg structure forms in wich the acidic and basic sites are in atomic proximity, which reduces the activation energy of consecutive reactions that lead to butadiene formation.

In this study we prepared a partly silica-covered MgO catalyst, using the Chung's method. We characterized the structure, acid-base properties, and catalytic activity when converting ethanol and an ethanol/acetaldehyde mixture. Our study shows that MoO_2 on the surface of MgO-SiO_2 can promote ethanol conversion, the acetaldehyde formation, but not the butadiene/butanol selectivity. Acetaldehyde co-fed with reactant ethanol establishes more favorable conditions for obtaining afore mentioned C_4 products regardless of the presence or absence of metal or metal oxide promoter.

2. Experimental

2.1. Catalyst synthesis

The wet-kneaded MgO-SiO_2 catalysts were prepared from $Mg(OH)_2$ and Cab-O-Sil® fumed silica using the method described by Chung et al. [38]. The $Mg(OH)_2$ was precipitated from a 1 M magnesium nitrate solution ($Mg(NO_3)_2{\cdot}6H_2O$, Alfa Aesar, ACS, 98–102 %) at pH 12. The pH of the solution was adjusted via the dropwise addition of a 2 M NaOH solution. After aging for one hour, the precipitate was separated by centrifugation, washed five times with distilled water, and dried at 120 °C overnight. A mixture of $Mg(OH)_2$ and SiO_2, with a 2 to 1 Mg to Si atomic ratio, was suspended in a 100-fold excess of distilled water and the initial pH of the solution (10.4) was adjusted to 11.4 with a 12.5 wt % ammonia solution. Under these conditions, a significant portion of SiO_2 is in solution while a significant portion of MgO is in the solid phase. Then, the mixture was kneaded for two hours using a high-shear mixer. The solid part, separated by centrifugation, was dried overnight at 120 °C. It was then heated at a rate of 5 °C min^{-1} to 500 °C and calcined for five hours. The MgO-SiO_2 sample thus prepared is designated as WK catalyst.

Molybdenum-containing catalysts were prepared by impregnating the wet-kneaded MgO-SiO_2 with ammonium paramolybdate ($(NH_4)_6Mo_7O_{24}{\cdot}4H_2O$, Reanal, Hungary) solution until the desired MoO_3 content of 2 or 5 wt % was achieved. For each gram of the mixed oxide, 10 cm^3 of the appropriate concentration of paramolybdate solution was added. The water content was then evaporated, and the solid residue was dried at 120 °C overnight. Next, it was heated at a rate of 5 °C min^{-1} to 500 °C and calcined for five hours. These preparations are designated as 2MoWK and 5MoWK catalysts.

2.2. Characterization of catalysts

The compositions of the MgO-SiO_2 and Mo-containing samples were determined by inductively coupled plasma optical emission spectroscopy (ICP-OES) using a SPECTRO GENESIS spectrometer (SPECTRO Analytical Instruments GmbH, Kleve, Germany).

The catalysts were characterized using nitrogen adsorption-desorption isotherms measured at −196 °C with a Thermo Scientific™ Surfer automatic volumetric adsorption apparatus (Thermo Fisher Scientific, Waltham, MA, USA). Prior to the measurements, the samples were pretreated in a vacuum at 250 °C for 120 min. The Brunauer–Emmett–Teller (BET) method was used to calculate the specific surface area. The Barrett–Joyner–Halenda (BJH) method was used to calculate the pore size distribution. The micro- and mesopore volumes

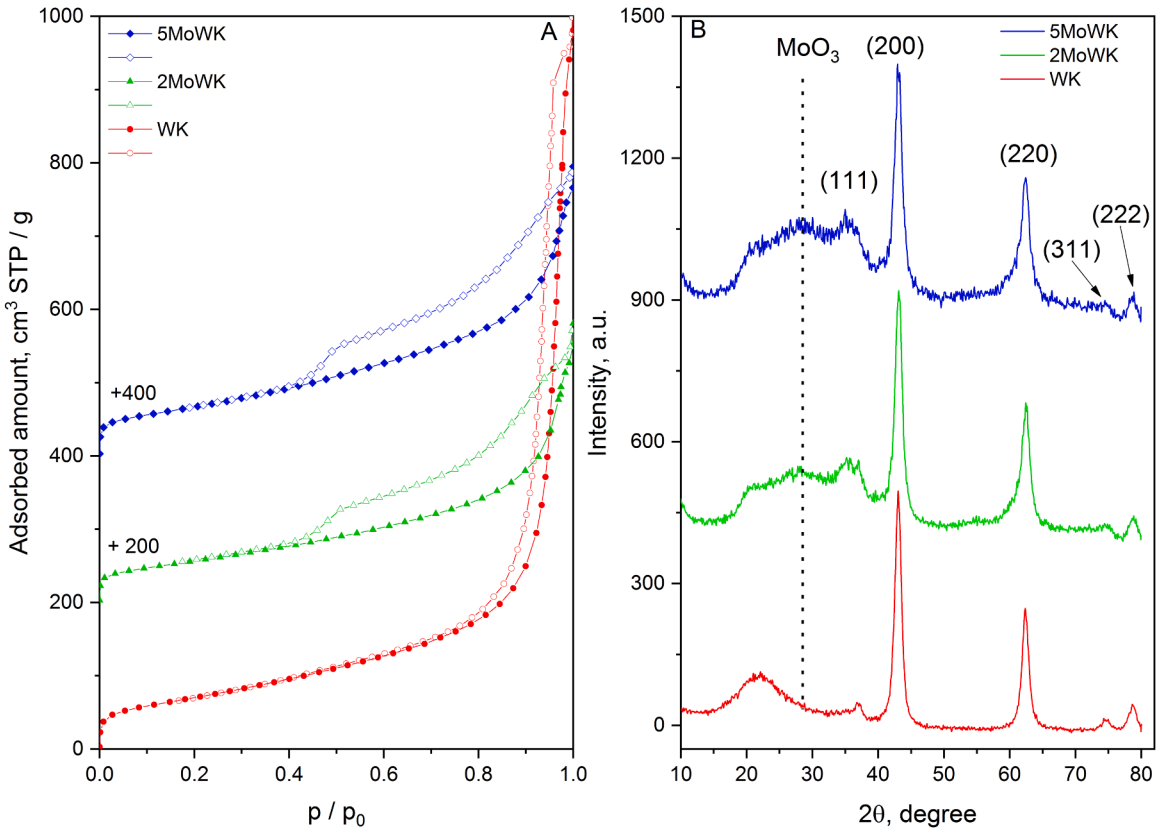

Fig. 1. (A) Nitrogen physisorption isotherms of the catalysts, with the adsorption branch marked with full symbols and the desorption branch marked with open symbols. (B) XRD patterns of the catalysts. The intensities of the lines are normalized to the periclase line (200) of the WK sample.

were determined using the Gurvich method.

The powder X-ray diffraction (PXRD) patterns of the catalysts were recorded using a Philips PW1810/3710 diffractometer (Malvern Panalytical B. V., Amelo, Netherlands) at room temperature, between 5° and 80° (2θ), with a step size of 0.04° and a dwell time of 0.5 s per step. Monochromatized CuKα radiation (λ = 0.15418 nm) was used with an excitation voltage of 40 kV and a current of 35 mA.

Scanning electron microscope (SEM) images were obtained with a Thermo Fisher Scientific Apreo C (Thermo Fisher Scientific, Waltham, MA, USA). The elemental map of the samples was recorded using energy-dispersive X-ray spectroscopy (EDX). Microscopic images were obtained with a current of 40 mA and an acceleration voltage of 20 kV.

The acid-base properties of the catalysts were characterized using temperature-programmed desorption (TPD) of adsorbed ammonia (NH_3) and carbon dioxide (CO_2). Approximately 200 mg of catalyst from the 0.315–0.650 mm sieve fraction was loaded into a U-shaped quartz tube reactor with an internal diameter of 4 mm. The catalyst was then activated at 500 °C for one hour with a 30 mL min^{-1} oxygen flow and cooled to room temperature within the flow. After evacuation, the sample was exposed to CO_2 to characterize basicity or NH_3 to characterize acidity, each at 13.3 kPa for 15 min. To remove weakly adsorbed molecules, the sample was evacuated for 15 min, after which it was heated to 500 °C at a rate of 10 °C min^{-1} in a helium flow of 21.4 mL min^{-1}. The gas flow leaving the catalyst was first passed through an acetone/dry ice trap and then through a thermal conductivity detector (TCD). The catalyst was held at the final temperature for 30 min. The NH_3-TPD measurement protocol included a 30 min isothermal step at 150 °C to separate the desorption from the sorption sites of weak and medium acid strengths. The final temperature of 500 °C was maintained for one hour. The TPD curves were integrated, and the amount of desorbed gas was calculated based on calibration values.

Qualitative characterization of acidic sites was performed using pyridine adsorption FTIR measurements. Prior to taking the measurements, the self-supporting wafers were activated in a hydrogen or oxygen stream at 450 °C for one hour. The sample was cooled to 200 °C in the applied gas stream. After 30 min of evacuation at 200 °C, the sample was exposed to pyridine at a pressure of 666 Pa for 30 min. Spectra were recorded at 100, 200, 300, and 400 °C after 30 min of evaporation at each temperature.

Temperature-programmed hydrogen reduction (H_2-TPR) measurements were used to characterize the oxidation states of the Mo in the catalysts. The same equipment, catalyst loading, and pretreatment were used as for the TPD measurements. At room temperature, the O_2 flow used for pretreatment was switched to a 30 mL min^{-1} flow of a 10 % H_2/N_2 gas mixture. After a stabilized TCD signal was attained, the sample was heated to 800 °C at a rate of 10 °C min^{-1} and held there for one hour. The gas stream leaving the quartz tube reactor passed through a trap containing liquid nitrogen to freeze the formed water and then through a TCD to measure the H_2 concentration as a function of temperature. The amount of H_2 consumed for reduction was calculated based on the calibration value.

Thermogravimetric mass spectrometric (TG-MS) characterization of the 5MoWK catalyst was carried out using a Setaram Labsys Evo TG-DTA/DSC (EGA) system connected to a Pfeiffer Vacuum OmniStar MS gas analyzer (Pfeiffer Vacuum GmbH, Asslar, Germany). Measurements were taken in He and in synthetic air at temperatures ranging from 25 to 800 °C. The gas flow rate was 80 mL min^{-1} while the heating rate of 5 °C min^{-1}. The results were evaluated and processed using the Calisto Processing 2.092 AKTS program.

Ultraviolet-visible (UV–Vis) spectrophotometric measurements were performed using a Thermo Scientific Evolution 300 instrument equipped with a Praying Mantis diffuse reflectance unit to determine the UV

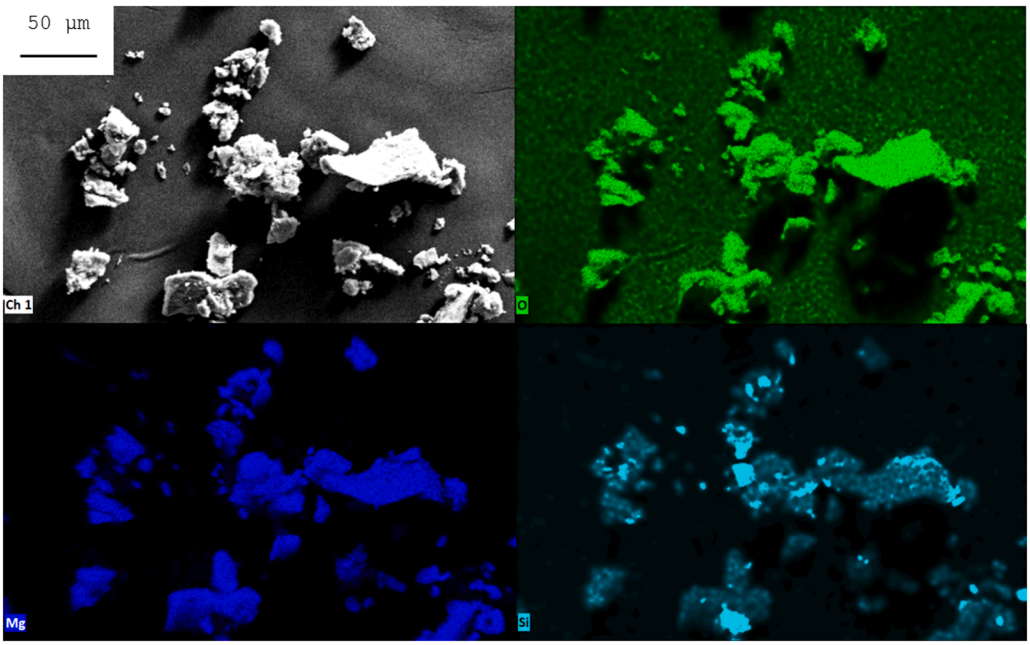

Fig. 2. SEM image of sample WK and spatial distribution of O, Mg and Si elements determined by EDX mapping method.

absorption edge energies of the Mo-catalysts. This instrument allows samples to be pretreated at high temperatures and pressures. For the background recording, 99.998 % pure barium sulfate (Alfa Aesar $BaSO_4$) was used. Spectra were recorded within the 200–800 nm wavelength range with a resolution of 2 cm^{-1}. To remove the adsorbed water the finely powdered sample was heated in the measuring cell to 450 °C in an oxygen stream. After 30 min, a spectrum was recorded at this temperature. Another spectrum was recorded after the sample had been cooled back to room temperature. To eliminate self-absorption and other interfering effects, the samples were diluted with Alfa Aesar $BaSO_4$ to such an extent that the Kubelka–Munk function, $F(R_\infty)$, calculated from the reflectance values, met the $F(R_\infty) < 1$ condition. The edge energy (Eg) of the allowed transitions was determined by fitting a straight line to the low-energy rise of the $F(R\infty)h\nu^2$ vs. $h\nu$ plot, where $h\nu$ represents photon energy [42].

2.3. Catalytic test reactions

The temperature and space-time dependence of the conversion and selectivity was studied at atmospheric pressure using either 15 vol % ethanol/He or 13.5 vol % ethanol/15 vol % acetaldehyde/He gas mixture as reactant. Experiments were carried out also with 15 vol % acetaldehyde/He.

A tubular, flow-through microreactor made of glass with an internal diameter of 8 mm was used. Prior to each measurement 0.5 g of catalyst was activated in situ in the reactor in a 15 $cm^3 \cdot min^{-1}$ oxygen flow at 450 °C for 30 min. A Gilson 307 type HPLC pump was used to introduce the liquid ethanol, acetaldehyde, or ethanol/acetaldehyde reactant into an evaporation chamber, which was held at 120 °C temperature. From the chamber the vapor mixture was flushed into the reactor with a helium flow.

The reactor outlet was connected to an on-line Shimadzu GC-2010 type gas chromatograph (GC, Shimadzu Corp., Kyoto, Japan) with a pipeline kept at 120 °C to prevent the condensation of any product before the sample of the product mixture entered the GC. The GC operated with two columns and two flame ionization detectors (FIDs). The oxygen-containing products were analyzed using a PoraPlot Q (50 *m* × 0.32 mm × 10 µm) column. The hydrocarbon products were analyzed using a KCl-deactivated CP-Al_2O_3 (50 *m* × 0.32 mm × 5 µm) column. The product mixture leaving the reactor and the GC was collected in an ethanol/dry ice trap and analyzed by Shimadzu GCMS-QP2010SE type GC–MS instrument equipped with ZB-WAXplus (60 m, 0.32 mm, 0.5 µm) column. The system was calibrated using separate samples of the reactants and main products. Conversion was calculated as the relation of the number of reactant moles consumed in the reaction and the number of moles fed in the reactor. The selectivity was obtained as the ratio of the number of carbon atoms of a given product to the total number of carbon atoms in all products.

3. Results

3.1. Composition and structural properties of the catalysts

The elemental composition of the samples is consistent with the amounts of reactants used to prepare them (Table S1).

The nitrogen physisorption isotherms of the catalysts are shown in Fig. 1A. The specific surface area (SSA), calculated by the BET method, is 200–250 m^2/g. According to the IUPAC classification [43], the isotherms are type IV, indicating that the samples are mesoporous. The hysteresis loop of the WK sample is H1 type and shows a regular pore size distribution with a maximum pore diameter of ~31 nm. After impregnation of molybdenum oxide, the isotherms of both catalysts change to H3 type, indicating a broadening of the original pore size distribution. The explanation for the widening is that the MoO_3 nanoparticles are incorporated into the pores of the WK and partially or even completely block them. In the sample with higher molybdenum content, larger nanoparticles are formed, which result in the formation of a pore system that provides a larger specific surface area calculated using the BET method.

After impregnation with MoO_3, a broad line appears in the X-ray diffractograms of 2MoWK and 5MoWK between 20° and 35° 2Θ values [44], with slightly higher intensity in the sample with higher molybdenum content. The broadening of the lines indicates that the size of the MoO_3 crystallites is small. Thus, it is not possible to determine whether an orthorhombic or hexagonal form has formed [45]. Valihura et al. identified the hexagonal form on the Mo/MgO-Al_2O_3 catalyst at a significantly higher molybdenum trioxide (MoO_3) content of 15.7 wt %. The lines of the periclase form of MgO (2Θ = 42.95° [200], 62.36° [220], etc.) and the broad line of amorphous SiO_2 (2Θ = 23°) can be identified in all three samples.

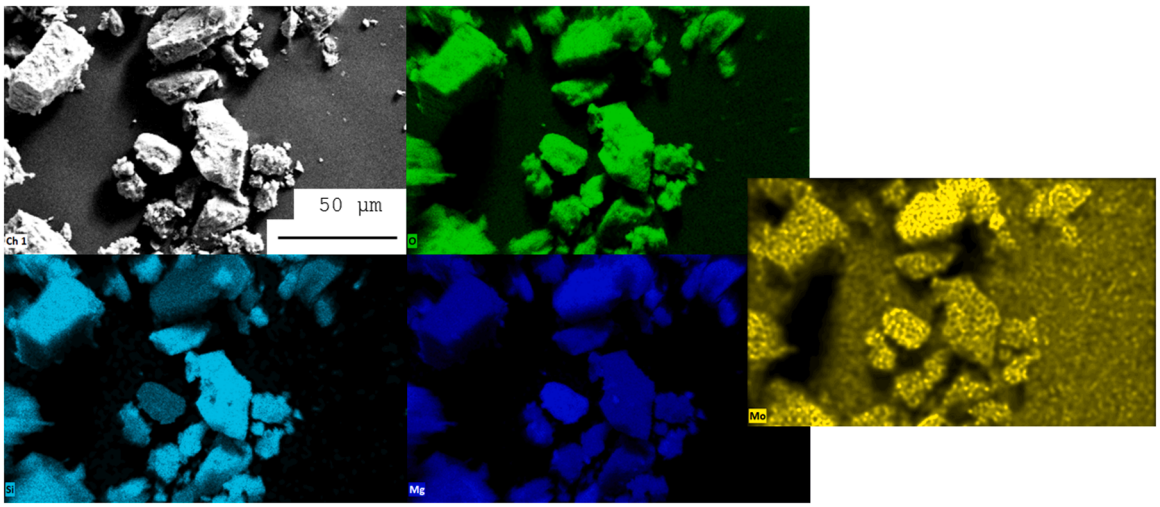

Fig. 3. SEM image of sample 2MoWK and spatial distribution of O, Mg, Si and Mo elements determined by EDX mapping method.

Table 1
The textural and acid-base properties of the catalysts.

Catalyst	SSA[a] $m^2 \cdot g^{-1}$	PV[b] $cm^3 \cdot g^{-1}$	PD[c] nm	Mo density atoms·nm^{-2}	c_a weak[d] $\mu mol \cdot g^{-1}$	c_a medium[d] $\mu mol \cdot g^{-1}$	c_b[e] $\mu mol \cdot g^{-1}$
WK	250	1.48	31.4	-	134	69	108
2MoWK	200	0.50	-	0.42	196	159	71
5MoWK	238	0,54	-	0.88	129	101	41

[a] Specific surface area, determined by BET method.
[b] Pore volume, determined by Gurvich method.
[c] Most frequent pore diameter. calculated by BJH method.
[d] Concentration of acidic sites, determined by NH_3-TPD method.
[e] Concentration of basic sites, determined by CO_2-TPD method.

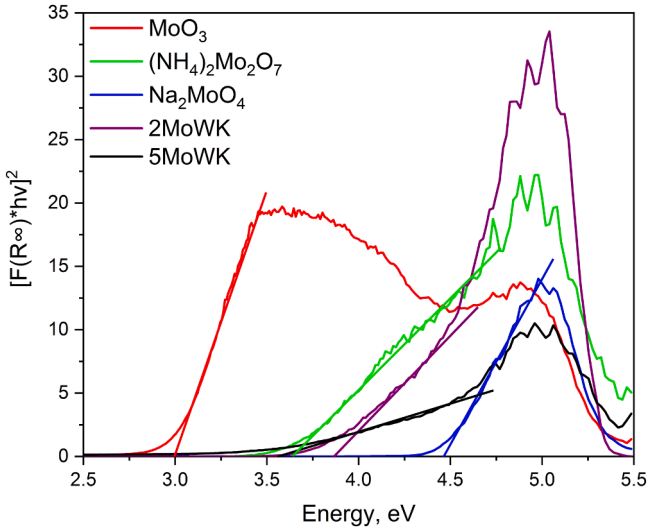

Fig. 4. Determination of the UV adsorption edge energies of the standard compounds (Na_2MoO_4, $(NH_4)_2Mo_2O_7$, MoO_3) and the 2MoWK and 5MoWK catalysts.

Scanning electron microscopic (SEM) images and corresponding elemental maps show that MoWK catalysts comprise SiO_2-covered MgO particles with molybdenum distributed evenly on their surfaces. (Figs. 2 and 3).

The molybdenum densities of the samples were calculated using the ratio of molybdenum content to specific surface area and found to be 0.43 and 0.88 Mo_{atoms} nm^{-2} for the 2MoWK and 5MoWK samples, respectively (Table 1.). According to Thielemann et al. [46] the formation of surface molybdenum forms is independent of the chosen synthesis method at such Mo densities. It is known that molybdenum can be present on the surface of oxide supports in polyoxomolybdate anions having different degrees of polymerization [47]. These forms can easily be identified using UV–Vis spectrophotometry. To achieve this, the edge energy (Eg) of the allowed transitions must be determined. The spectra recorded for the catalysts and standard materials in their dehydrated state are shown in Fig. 4. In the Na_2MoO_4 structure the molybdenum (VI) atoms are isolated (i.e., the Mo atoms have no Mo neighbor). In the $(NH_4)_2Mo_2O_7$ standard represents the structures containing molybdenum (VI) dimer (i.e., the Mo atoms have one Mo neighbor). In the MoO_3 standard, the molybdenum(VI) atoms are in a bulk phase (i.e., the Mo atoms have five Mo neighbors). Fig. 4 shows that, due to their low molybdenum content, the catalyst samples exhibit Eg values between those of isolated and dimeric molybdenum structures [48]. Fig. 4 also shows that the slope of the fitted line (i.e., the Tauc coefficient) is much steeper for the 2MoWK sample than for the 5MoWK sample. The value of the Tauc coefficient is known to depend on electronic delocalization and structural order and it decreases with increasing crystallinity [49]. This finding also indicates that the degree of ordering of molybdenum in the 2MoWK sample is higher than in the 5MoWK sample. This can be explained by the existence of several molybdate structures at higher molybdenum contents. As shown in Figure S1, the H_2-TPR measurements indicate that reducing molybdenum in the 2MoWK sample is more challenging than in the 5MoWK sample. It starts at a higher temperature, and while the 5MoWK sample has a hydrogen consumption of 2.43 H/Mo up to ~660–670 °C, the 2MoWK sample has a hydrogen consumption of only 1.37. Additionally, the total reducibility of the 2MoWK sample is slightly lower than that of the 5MoWK sample (H/Mo ratio is 4.93 vs. 5.10). Arena and Parmaliana [50] used H_2-TPR

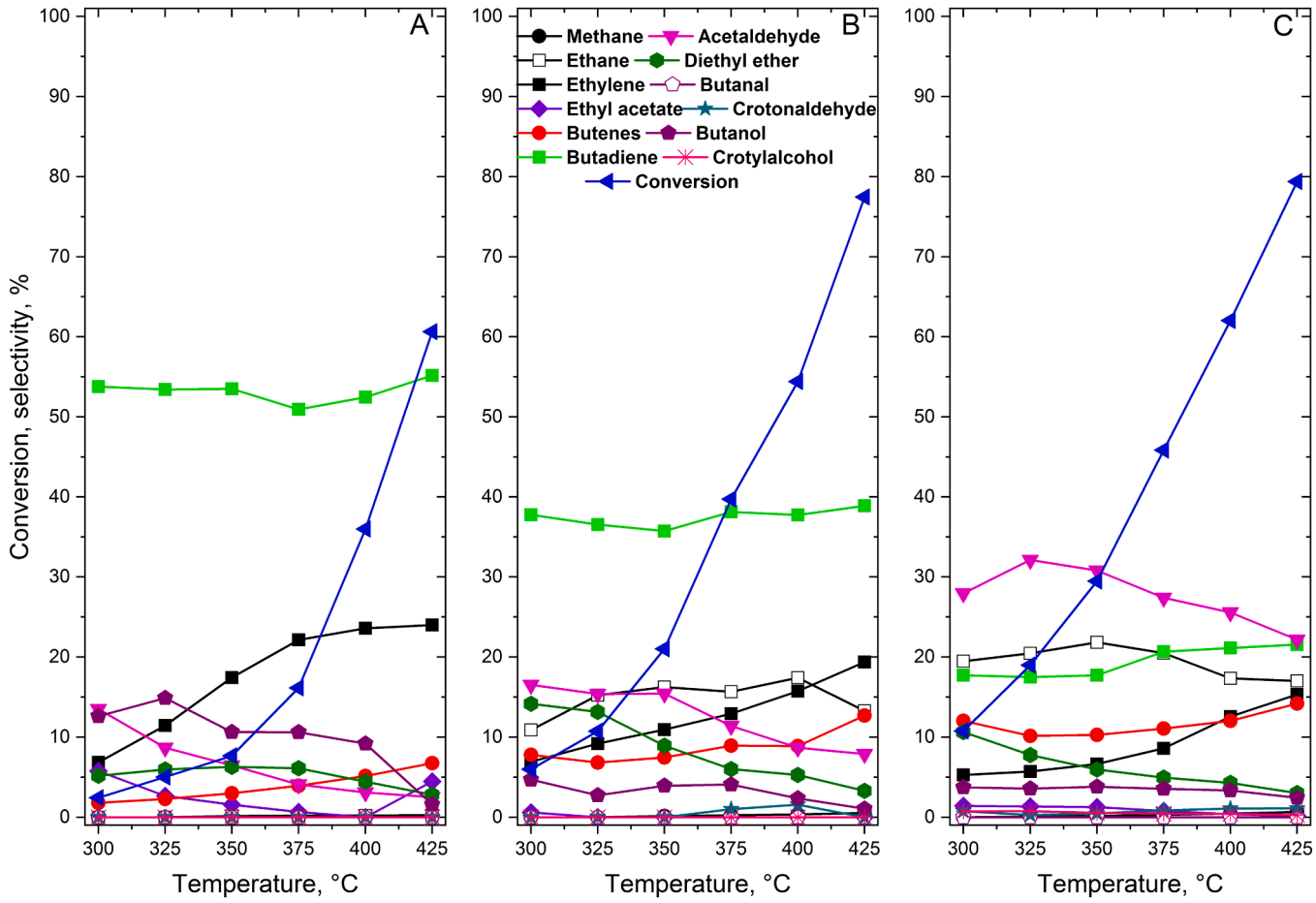

Fig. 5. The temperature dependence of the ethanol conversion on WK (A), 2MoWK (B) and 5 MoWK (C) catalysts. The reaction conditions used were:~15 % ethanol/He; 0.5 g of catalyst; 1 $g_{ethanol} \cdot g_{cat}^{-1} \cdot h^{-1}$; a total flow rate of 30 ml/min.

measurements on MoO_3/SiO_2 catalysts and found that the reducibility of different molybdenum forms decreases in the following order: polymolybdates > MoO_3 crystallites > isolated molybdates. Thus, the results of the H_2-TPR measurements corroborate the UV–Vis findings, which indicate that the 2MoWK sample primarily consists of isolated molybdates, while the 5MoWK sample contains a mixture of isolated molybdates and polymolybdate forms.

3.2. Acid-base properties of catalysts

It is widely accepted that the activity in the ethanol coupling reactions is controlled by the acid-base properties of the catalyst. However, there is still no clear correlation between the surface characteristics determined by NH_3- and CO_2-TPD measurements and the product distribution [39]. The efficiency of the ETBD reaction is significantly influenced by the number, strength, and spatial structure of the catalyst's acid and base sites. For MgO-SiO_2 catalysts, acid sites form along Mg-O-Si bonds. Base sites, on the other hand, are assigned to MgO. As shown in Table 1 and Figure S2, the catalysts' acidity increased and their basicity decreased after molybdenum oxide impregnation compared to the initial WK. MoO_3 is a Lewis acid, so its presence alone increases the catalyst's acidity. New Si-O-Mo bonds form during impregnation and subsequent heat treatment, further increasing the acidity of the samples. As shown in Table 1, the number and strength of the acid sites are highest in the 2MoWK sample. This can be explained by the fact that this sample contains primarily isolated molybdates, which form more Si-O-Mo bonds than polymolybdates do. In polymolybdates, most of the molybdenum atoms are part of Mo-O-Mo chains and cannot form Mg-O-Si bonds. The decrease in basicity due to molybdenum impregnation occurs because the acidic heptamolybdate ions react with the basic sites of WK, reducing the number of basic sites. This also explains why impregnating with a larger amount of molybdenum reduces WK's basicity more. The results of pyridine adsorption FT-IR measurements (Figure S3) demonstrate that the 5MoWK sample exclusively contains Lewis acid sites in both its oxidized and reduced forms.

3.3. Results of catalytic test reactions

Fig. 5 shows the temperature dependence of ethanol conversion. At each temperature, conversion was higher with the MoWK catalysts than with the WK catalyst. Butadiene selectivity remained nearly constant within the tested temperature range. It was approximately 55 % for the WK catalyst, and approximately 40 % and 20 % for the 2MoWK and 5MoWK catalysts, respectively. Butanol selectivity was much lower than butadiene selectivity and was lower at lower Mo content and higher reaction temperature. In contrast, the acetaldehyde selectivity of the Mo catalysts was significantly higher than that of the WK catalyst. More ethane and less ethylene were formed on the MoWK catalysts than on the WK catalyst.

Butanal and crotyl alcohol are possible intermediates in the formation of butadiene and/or butanol. However, no butanal was found in any of the product mixtures. The MoWK catalysts had somewhat higher selectivity for crotyl alcohol than the WK catalyst, but it was still <1 %, even at the highest applied reaction temperature.

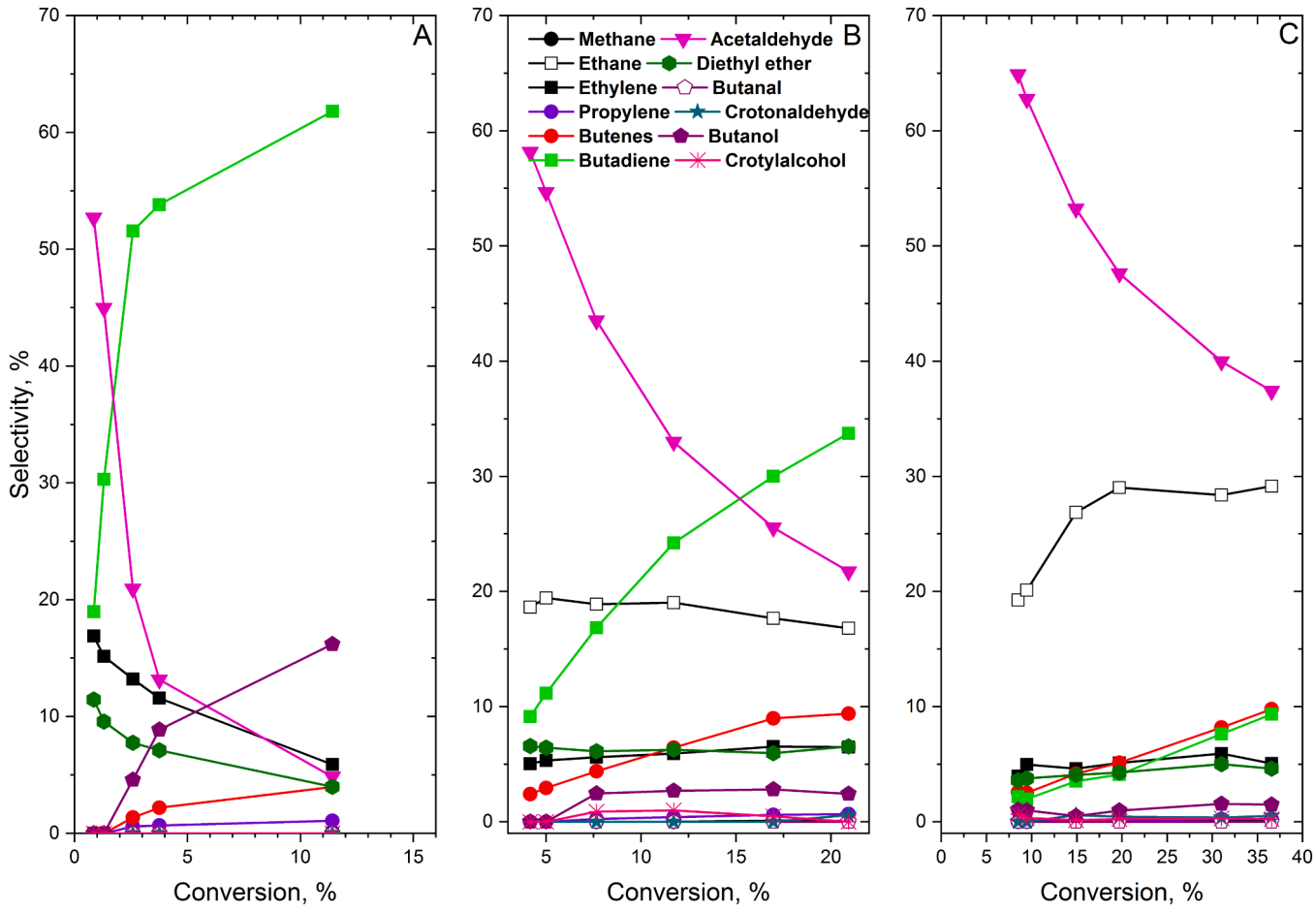

Fig. 6. The effect of conversion on product selectivity at 325 °C in reaction of ethanol on WK (A), 2MoWK (B) and 5MoWK (C) catalysts. Different conversions were achieved by varying the space velocity. The reaction conditions used were: ~15 % ethanol/He; 0.5 g of catalyst; 0.33–6 $g_{ethanol} \cdot g_{cat}^{-1} \cdot h^{-1}$; a total flow rates between 10 and 180 ml/min.

Butenes were present in the product mixtures at a concentration greater than 10 %. Minor amounts of butane, propane, and propylene were also detected (not shown).

The conversion of ethanol was studied as a function of space-time at 325 °C. Product selectivities are represented as a function of conversion (Fig. 6). At low conversions, acetaldehyde was the main product. At higher conversions, acetaldehyde still formed with high selectivity on Mo-containing catalysts. This indicates that a large fraction of the primary aldehyde product did not participate in further reactions. On the 5MoWK catalyst, ethane was the second main product. It is also important to note that crotonaldehyde and crotyl alcohol were only detected with a selectivity of <0.5 % at the highest conversions. The butanol selectivity was higher with the catalyst that contained less Mo and became the second main product with the Mo-free WK catalyst at higher conversions.

The effect of space-time on ethanol conversion was also studied at a temperature of 375 °C (Figure S4). Despite the higher conversion rates, the selectivity curves for the Mo-containing catalysts were like those observed at 325 °C. However, the activity of the WK catalyst was different. At high space-times (low WHSV, high conversions), the acetaldehyde selectivity remained below 20 %, while the butadiene selectivity was significantly higher than at 325 °C. At lower space-times (high WHSV, lower conversions), the higher temperature no longer affected the product distribution. The selectivity was approximately 1 % for crotyl alcohol and 0.5 % for crotonaldehyde across the entire examined space-time range.

Fig. 7 shows the product distribution resulting from the conversion of the acetaldehyde/ethanol mixture as a function of temperature. Acetaldehyde had no significant effect on the amount of converted ethanol (see Figs. 5 and 7). Note that acetaldehyde was a reactant and a possible product in these reactions. With the 5MoWK catalyst, negative acetaldehyde conversion was calculated because the product mixture contained more acetaldehyde than the feed (Figure S5). As shown in Fig. 7, the product distribution is distorted because the calculation did not account for the significant yet unknown amount of acetaldehyde that could have been produced. As an alternative extreme approach to addressing the selectivity problem, the total acetaldehyde content of the product mixture was used in the calculation (Figure S6). It can be concluded that acetaldehyde in the reactant mixture promoted the butadiene selectivity of the WK catalyst at temperatures between 350 and 425 °C. The positive effects of acetaldehyde were even higher on the butadiene selectivity of Mo-containing catalysts. Butanol was also obtained with higher selectivity from the conversion of the mixture than from the conversion of pure ethanol. It is important to note that crotonaldehyde formed with significant selectivity on the WK catalyst at low temperatures and that the condensation product, ethyl vinyl ether, also appeared (Fig. 7). The significant formation of crotonaldehyde was surprising because only trace amounts of crotonaldehyde were obtained from the conversion of pure ethanol on this catalyst (Fig. 5).

The conversion of the acetaldehyde/ethanol mixture was studied as a function of space-time at a temperature of 325 °C. Product selectivities were plotted against conversion (Figs. 8 and S5) and compared with corresponding results obtained using pure ethanol as the reactant (Fig. 6). At low conversions, ethyl vinyl ether and ethyl acetate appeared among the products. Acetaldehyde in the reactant mixture promoted the formation of butadiene on Mo-containing catalysts at longer space-times

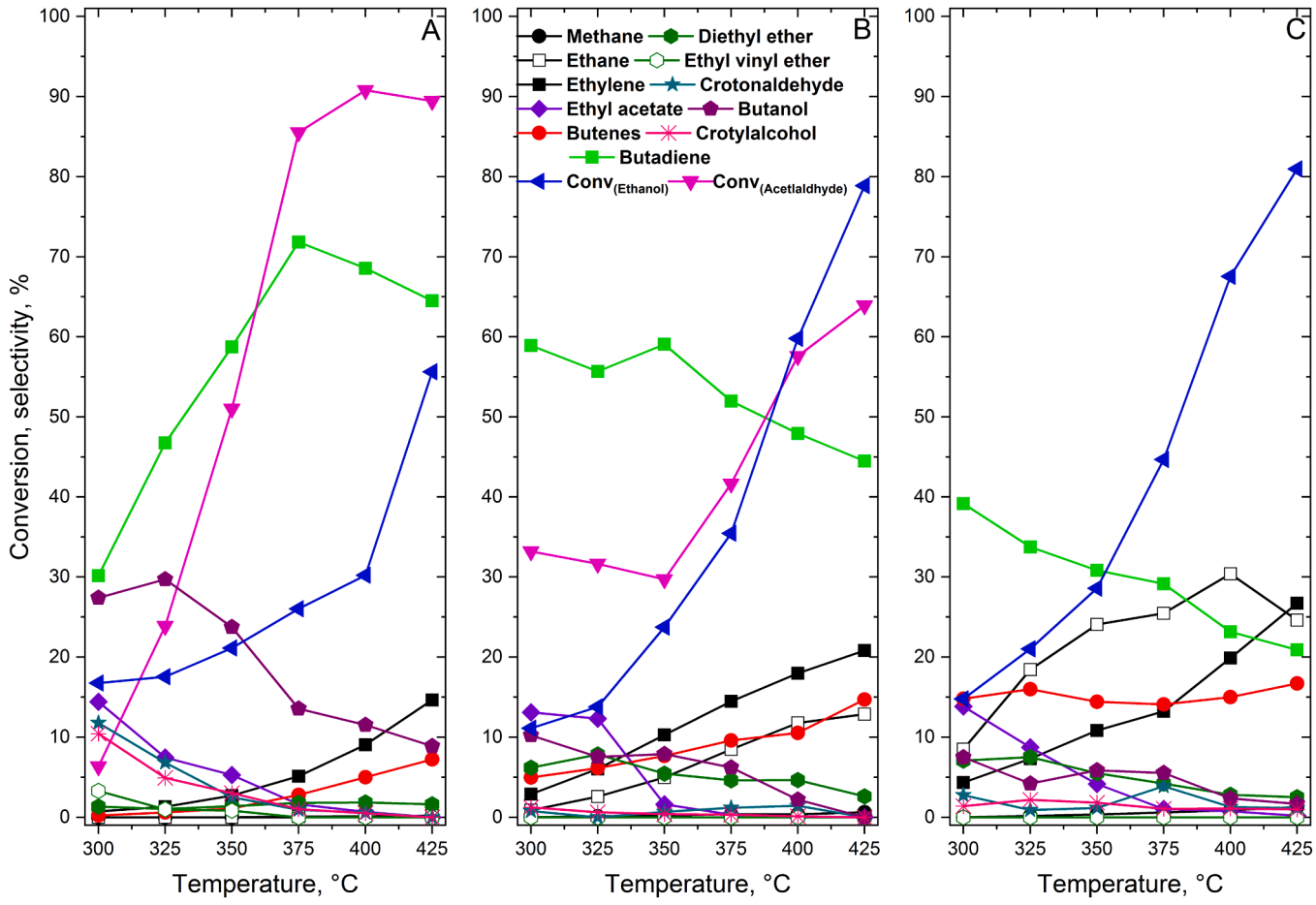

Fig. 7. The temperature dependence of the conversion of the ethanol/acetaldehyde mixture on WK (A), 2MoWK (B) and 5MoWK (C) catalysts. The reaction conditions used were:~13.5 % ethanol + 1.5 % acetaldehyde/He; 0.5 g of catalyst; 1 $g_{mixture} \cdot g_{cat}^{-1} \cdot h^{-1}$; a total flow rate of 30 ml/min.

while suppressing the formation of ethane. Crotyl alcohol and crotonaldehyde were also among the products; these products formed only in small amounts from pure ethanol. Acetaldehyde was present in significant amounts in the product mixture at the lowest conversions (WHSV of 6.0 $g_{reactant} \cdot g_{cat}^{-1} \cdot h^{-1}$), and its selectivity decreased with increasing conversion on all three catalysts (Figure S7).

The effect of space-time was also investigated at a temperature of 375 °C (Figures S8 and S9). It was found that the coupling reactions in the acetaldehyde/ethanol mixture were more facile than those in pure ethanol (see Figures S4 and S6). Despite the higher conversion rates, the selectivity curves for the Mo-containing catalysts were like those obtained at 325 °C (see Figs. 8 and S7). At low space-times, the selectivity of butadiene, butanol, crotonaldehyde, and crotyl alcohol was higher for the mixture than for pure ethanol. The acetaldehyde in the mixture suppressed the formation of ethyl vinyl ether and ethyl acetate. At higher space-times on Mo-containing catalysts, the selectivity of C_4 oxygenates decreased, and the proportion of ethane and butenes in the product mixture increased. The product mixture obtained with the WK catalyst at higher conversions contained virtually no acetaldehyde. In contrast, a significant amount of acetaldehyde was present in the product obtained using Mo-containing catalyst (Figure S7). These results suggest that Mo in the catalyst promotes acetaldehyde formation but not the participation of the aldehyde in further transformations.

At a reaction temperature of 375 °C the activity of the WK catalyst changed minimally over 24 h, whereas the activity of the Mo-containing catalysts varied significantly (Fig. 9). Conversion decreased more sharply with higher molybdenum content. Acetaldehyde selectivity increased significantly with both Mo-catalysts, while ethane selectivity decreased at varying rates depending on the Mo content. The selectivity of the other products remained almost unchanged.

Upon examining the reaction of pure acetaldehyde (15 vol %/He), it was found that crotonaldehyde was the main product for both the WK and 5MoWK catalysts, with selectivities of 93 % and 99 %, respectively (Figure S10). Acetaldehyde conversion on the WK catalyst varied between 25 and 30 %, while on the MoWK catalyst it varied between 18 and 20 % in the temperature range of 300 to 350 °C. The main by-products were ethanol and butanal.

3.4. *Characterization of spent catalysts*

The activity of the 5MoWK catalyst decreased rapidly. The results of H_2-TPR measurements showed hydrogen consumption of 5.1 H/ Mo for the fresh, oxygen-activated 5MoWK catalyst and 3.85 H/Mo for the used catalyst (Figure S1). Later number proves that the MoO_3 impregnated on the catalyst became partially reduced during the reaction. The value of 5.1 H/Mo substantiates that even up to 800 °C temperature the Mo^{6+} was not reduced completely to Mo^0.

The activity of the used catalysts could be fully recovered by activation in oxygen stream at 450 °C for 30 min. The TG-MS spectrum of the catalyst not used yet in reaction showed a peak corresponding to CO_2 evolution at 312 °C. This peak could result from the decomposition of some carbonate. A similar peak did not appear for the catalyst previously used in coupling reaction because the carbonate was already decomposed at the reaction temperature. The TG-MS results suggested that the activity of the 5MoWK catalyst could have been changed not only due to reduction of Mo^{6+} but was deactivated at least partly also by

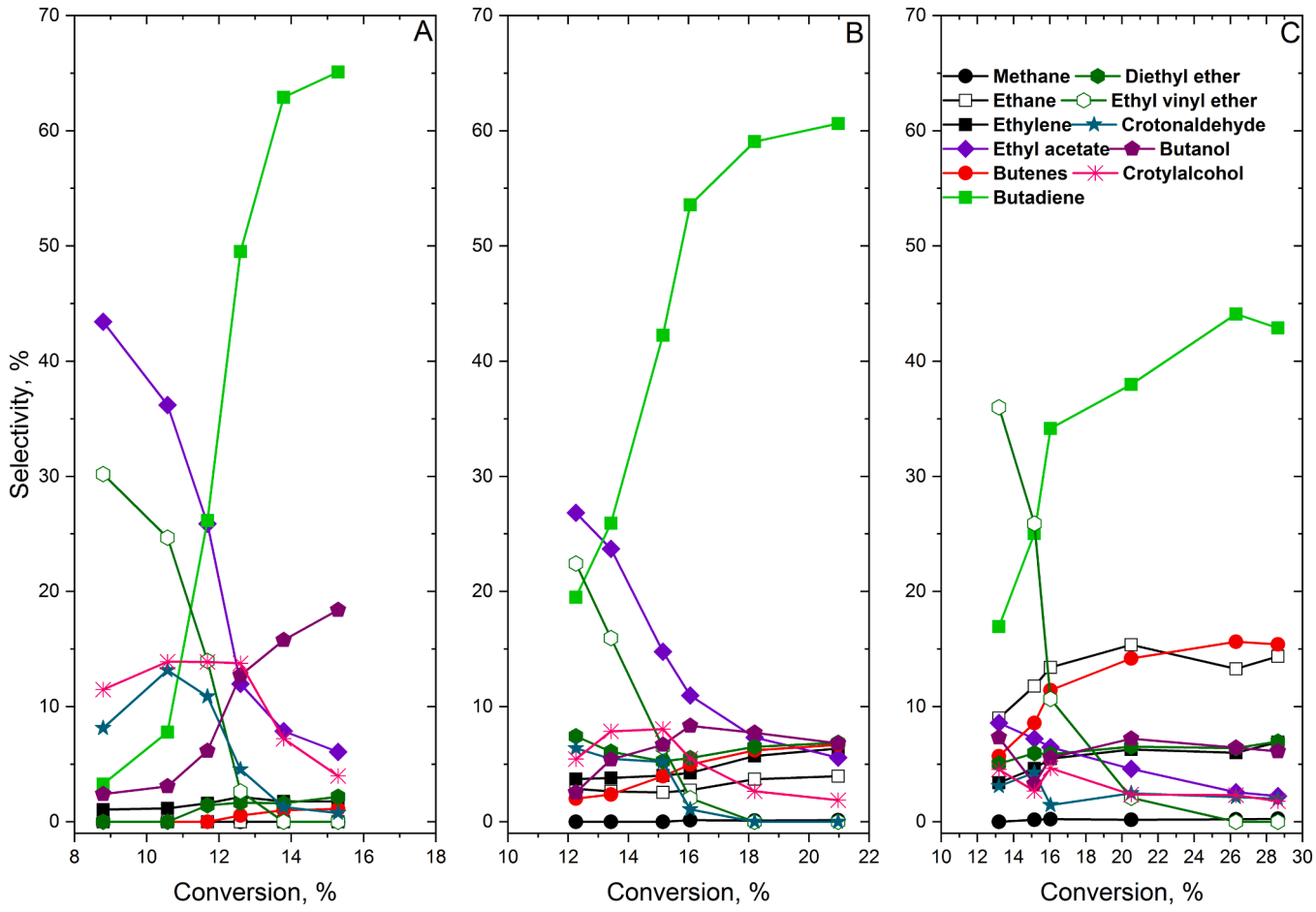

Fig. 8. The effect of conversion on product selectivity in reaction of ethanol/acetaldehyde mixture at 325 °C on WK (A), 2MoWK (B) and 5MoWK (C) catalysts. Different conversions were achieved by varying the space velocity. The reaction conditions used were: ~13.5 % ethanol + 1.5 % acetaldehyde/He; 0.5 g of catalyst; 0.33–6 $g_{mixture} \cdot g_{cat}^{-1} \cdot h^{-1}$; a total flow rates between 10 and 180 ml/min.

carbon deposition that could be removed by combustion in oxygen giving TG-MS peak at about 460 °C (Figure S11).

4. Discussion

Effect of acid-base paroperties. Previous results showed that the MgO phase is basic and plays an important role in the coupling reactions of ethanol and acetaldehyde, while, the Mg-O-Si bonds formed at the MgO-SiO_2 phase boundaries are acidic and have dehydration activity [40]. The basic and acidic surface sites co-operate in initiating the conversion of ethanol and acetaldehyde. Added transition metals were found to modify the catalytic activity of the MgO-SiO_2 mixed oxide. It became clear that the catalytic function of the metal component depends on the type of metal, its concentration, and its chemical state but the role of metal in steering the reaction is not yet fully understood. Mixed oxide MgO-SiO_2 was prepared by the wet kneading method and was used as catalyst (WK) and also as support to derive Mo/MgO-SiO_2 catalysts (MoWK). The pH applied during wet kneading resulted in a partly SiO_2-covered MgO structure, which has proven to be an effective ETBD catalyst (Fig. 5A) Following molybdenum impregnation, the catalysts exhibited increased acidity and decreased basicity This change in acid-base properties suppressed the coupling reactions; that is, the selectivity of butadiene and butanol decreased. Interestingly, however, the increase in acidity did not lead to an increase in the combined selectivity of the dehydrated products, i. e. ethylene and diethyl ether. The most notable effect of molybdenum doping is the increased amount of ethane and acetaldehyde in the product mixture.

Effect of MoO_3. Tian et al. [30] examined the ETBL reaction on MgO-Al_2O_3 supported MoO_3 catalyst. In these experiments, ethane formation was not observed. However, by poisoning the catalyst with acetic acid, the authors concluded that the amount of acetaldehyde in the product mixture had increased due to a decrease in the catalyst's basicity and the subsequent suppression of aldol condensation. Nakamura et al. [32] investigated the conversion of ethanol in mechanical mixtures of MoO_3/SiO_2 and MoO_2/SiO_2, both of which contained ~5.7 wt % molybdenum oxide. They found that acetaldehyde and ethane were formed in equimolar amounts in the sample containing reduced molybdenum (MoO_2), even at the initial stage of the reaction. Meanwhile, the ethylene selectivity is around 1 %. For the sample containing MoO_3, this equilibrium is reached after nine hours, with lower selectivities for ethane and acetaldehyde, accompanied by the formation of a significant amount of ethylene (~36 % selectivity). Based on these results, they concluded that ethane and acetaldehyde are produced in one step from a single intermediate formed by the rearrangement of two ethanol molecules adsorbed on two adjacent metal cation–oxygen anion pairs on reduced molybdenum oxyde. Ethane formation was also observed in our experiments, and it was evident that the amount of ethane produced increased with increasing molybdenum content. In our experiments, ethane formation begins in the initial stage of the reaction. This can be explained by the fact that the MoO_3 present in a higher dispersion on the supported catalyst is reduced more easily than the MoO_3 in the bulk phase in the experiment described above. Stability measurements conducted over 24 h revealed that the conversion on molybdenum-containing catalysts decreases continuously (Fig. 9). As

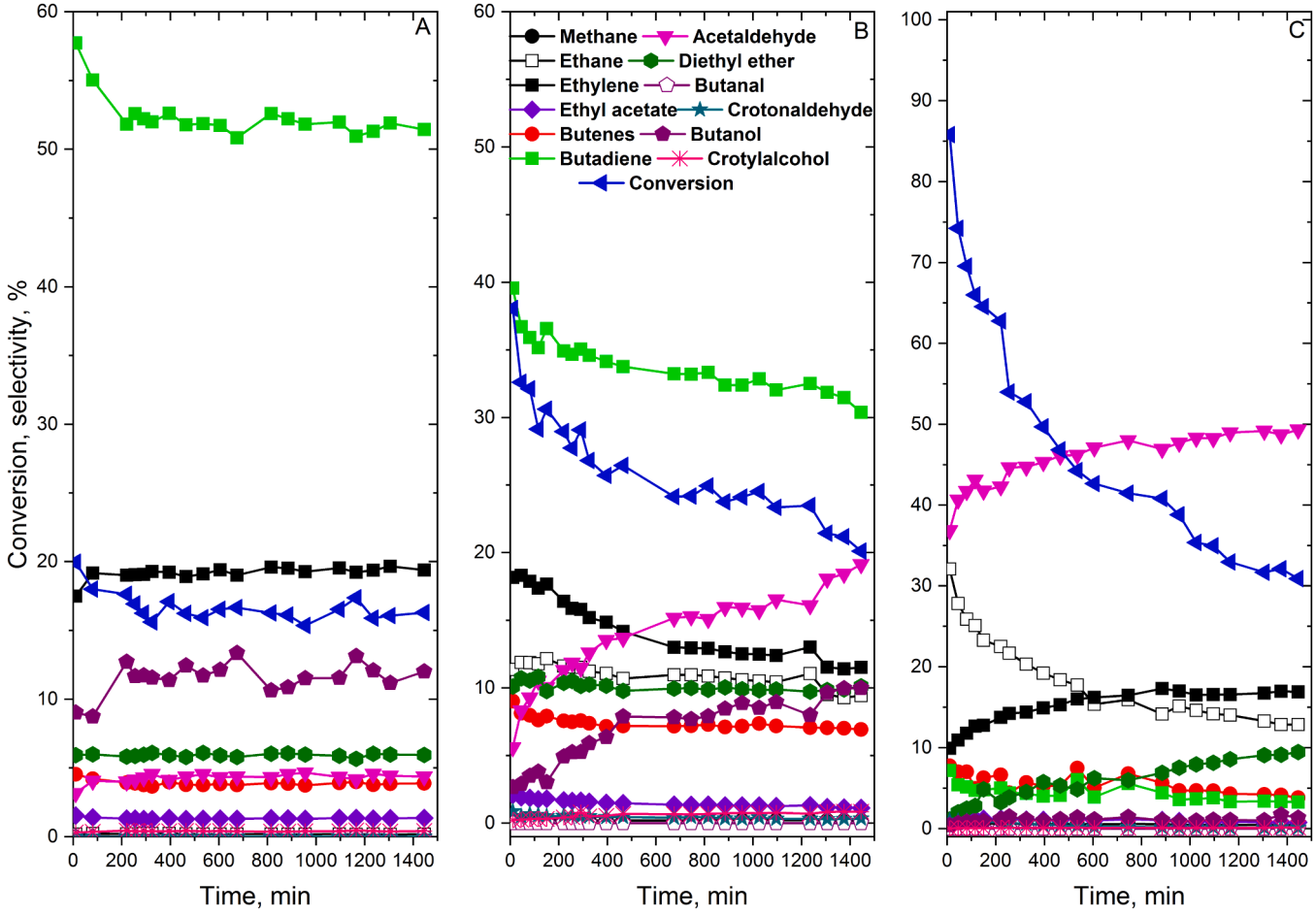

Fig. 9. The effect of time on stream at 375 °C on the ethanol conversion on WK (A), 2MoWK (B) and 5MoWK (C) catalysts. The reaction conditions used were:~15 % ethanol/He; 0.5 g of catalyst; 1 $g_{ethanol} \cdot g_{cat}^{-1} \cdot h^{-1}$; a total flow rate of 30 ml/min.

the conversion drops, the selectivity of butadiene on the 2MoWK catalyst decreases, while that of acetaldehyde increases. The increase in acetaldehyde selectivity on the 5MoWK catalyst is accompanied by a decrease in ethane selectivity. In other words, the coupling reactions are suppressed on both catalysts, even though there is a large quantity of acetaldehyde present in the system. On the 5MoWK catalyst, the coupling according to Reaction 1 should be considered.

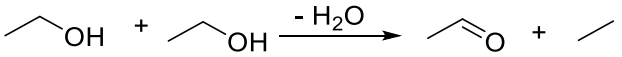

(1)

One might ask whether the molybdenum oxidation number is significant because it forms a Mo^{6+}/Mo^{4+} redox cycling system, which enhances the dehydrogenation of ethanol. This is highly unlikely because the reaction occurs in a reducing medium. This means that either the ethanol itself or the hydrogen produced during butadiene formation can reduce the molybdenum. Because there is no oxidizing agent in the system, the partially reduced molybdenum cannot be reoxidized, thus a redox cycle cannot develop. In summary, according to Nakamura et al. [32] the effect of MoO_3 can be interpreted as the reduction of molybdenum, which leads to a change in the reaction mechanism. That is, while the main reaction in the sample containing Mo^{6+} is the dehydrogenation of ethanol to acetaldehyde, after the partial reduction of molybdenum, the disproportionation of two ethanol molecules to ethane and acetaldehyde becomes the determining reaction. This change is the result of altered ethanol adsorption conditions.

Effect of acetaldehyde co-feeding. Santos et al. [51] concluded that the high Mg content of the Mg-Al-Si catalyst promoted the dehydrogenation of ethanol to the acetaldehyde intermediate, which readily underwent aldol condensation at the acid-base active sites of the support. However, the aldol mechanism is also strongly questioned as the only possible form of ethanol coupling [24,26,28]. To clarify the role of acetaldehyde in the reaction we studied the reaction of an ethanol/acetaldehyde mixture in which acetaldehyde (or an acetaldehyde-like intermediate) does not form in situ, but enters the reaction network as a whole molecule. As shown in Fig. 5, the WK catalyst produces butadiene with stable selectivity of 55 %, while relatively small amounts of acetaldehyde are formed. The butanol selectivity of 10–15 % can be explained by the presence of a separate MgO phase. As can be seen in Fig. 7, the conversion of acetaldehyde in the ethanol/acetaldehyde mixture increases significantly only from 375 °C. In parallel, the selectivity of butadiene formation also increases. At lower temperatures, the selectivity of butadiene is significantly lower than in the reaction with pure ethanol, while condensation products appear that cannot be detected in the reaction with pure ethanol (crotyl alcohol, crotonaldehyde, ethyl vinyl ether). The first two products are intermediates that are well-known in the aldol condensation pathway for the conversion of ethanol to butadiene or butanol. They can be identified in the reaction of pure ethanol, especially crotonaldehyde, but only in small amounts. The most widely accepted explanation for this is that they are rapidly converted into the appropriate final product (butanol or butadiene) depending on the characteristics of the catalyst. This conversion occurs at such a high reaction rate that the products do not leave the catalyst surface, even during an extremely short residence time. The question arises as to how the $C = C$ double bond in crotonaldehyde and crotyl alcohol is hydrogenated in systems that do not contain a metal component? Although MPV reduction occurs easily on $MgO\text{-}SiO_2$ and

$MgO\text{-}Al_2O_3$ catalysts, molecular hydrogen cannot reduce the $C = C$ double bond or the carbonyl group. In contrast, the reduction of the double bond in ethanol/crotonaldehyde and ethanol/crotyl alcohol mixtures is achieved with high conversion using both catalysts (not yet published). These results suggest that ethanol is responsible for the hydrogenation of the $C = C$ double bond, but not via the H_2 released from it. Rather, it occurs through a transition state in which molecular hydrogen is not formed. In other words, hydrogenation occurs between the two co-adsorbed species: ethanol and crotonaldehyde or crotyl alcohol. Examining the molybdenum-containing samples shows that the MoO_3 additive does not promote butadiene formation. The basic idea was good in that the amount of acetaldehyde in the product mixture increased. However, this did not lead to an increase in the amount of coupled products. Instead, ethane formation came to the fore (see Eq. (1), above), while crotonaldehyde and crotyl alcohol were not detected on these catalysts.

This characteristic pattern was also maintained in the molybdenum-containing samples in the ethanol/acetaldehyde reaction, i.e. the proportion of acetaldehyde in the product mixture was high, the selectivity of ethane and butenes was high, and the intermediates of the aldol condensation pathway could not be detected. The only difference is that the selectivity of butadiene is increased compared to that found in the reaction with pure ethanol (mostly because acetaldehyde is not included in the denominator of the selectivity calculation). Examining the space-time dependence at two different temperatures (325 °C and 375 °C) for the reaction of pure ethanol (see Figs. 7 and S2), it can be seen that, as the residence time on the WK catalyst increases, acetaldehyde disappears from the products and the selectivity of butadiene increases. It can also be observed that, while it increases with increasing space-time at 325 °C, the selectivity of butanol decreases at 375 °C. In samples containing molybdenum, it can be seen that a significant proportion of the acetaldehyde does not undergo further reaction. Meanwhile, ethane appears among the products and the formation of butadiene and butanol is suppressed compared to the reaction of pure ethanol. When the ethanol/acetaldehyde mixture is reacted at low conversions at 325 °C, products that are presumably the result of ethanol-acetaldehyde coupling (ethyl vinyl ether, Eq. (2)) and acetaldehyde-acetaldehyde coupling (ethyl acetate, Eq. (3)) appear, in addition to the intermediates of the aldol condensation pathway (crotyl alcohol and crotonaldehyde).

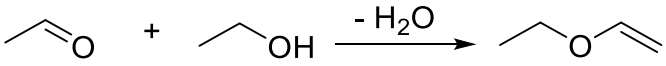

(2)

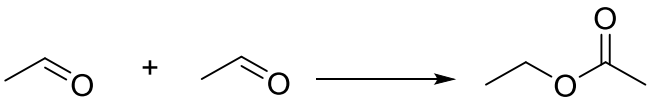

(3)

At higher space-time values, these products gradually disappear and a product distribution develops that is similar to that observed in temperature-dependent measurements at higher temperatures. Examining the results of the space-time dependence measurements performed at 375 °C (Figures S4 and S6), we can observe that the above-mentioned coupled products are formed in significantly smaller amounts at higher temperatures with high conversions at the same space-times, and disappear from the product mixture at lower space-times than at 325 °C.

It can also be seen that, while the selectivity of butanol increases with increasing space-time at 325 °C, this trend is reversed at higher temperatureThe most widely accepted theory for the mechanism of ethanol coupling reactions is that the carbon-carbon coupling occurs through the aldol condensation of two acetaldehyde molecules. In the reaction of pure ethanol, crotyl alcohol is the only intermediate found in the aldol condensation pathway at low conversions (low space-times), while significant amounts of butadiene and butanol are found in the products.

The product distribution changed when acetaldehyde was added to the reactant ethanol. The products of the acetaldehyde-acetaldehyde and acetaldehyde-ethanol (direct and semidirect pathways) couplings appeared. This suggests that acetaldehyde's reactivity as a reactant on the catalyst differs from its reactivity when produced from ethanol during the reaction. Coupled products can be formed in a similar way by rearrangement between molecules adsorbed on two adjacent active sites. An example of this is the formation of ethane and acetaldehyde, as mentioned above. Their formation is favored at lower temperatures and shorter residence times. Neither ethyl vinyl ether nor ethyl acetate can be intermediates in the formation of butadiene or butanol; both are formed in the direct condensation reaction shown above (Reactions 2 and 3). The following facts support the ethanol-ethanol and ethanol-acetaldehyde coupling mechanisms: (i) When pure acetaldehyde is added as a reactant, crotonaldehyde will appear among the products, in a way that is similar to the reaction of pure crotonaldehyde (See Figure S10). However, if it is formed during the reaction (i.e. during the reaction of pure ethanol), it will not appear. It is unlikely that this is a result of suppressing the Meerwein–Ponndorf–Verley reduction with 10 % acetaldehyde. (ii) At low conversion rates, butanol and butadiene are produced simultaneously. This requires the catalyst to both hydrogenate and dehydrate the crotyl alcohol. (iii) At 325 °C, butanol selectivity increases with increasing space-time as conversion increases. At 375 °C, however, it decreases. This is possible because at high temperatures the dehydrating activity increases and the hydrogenating activity decreases. Or at low temperatures (at lower ethanol conversions) the chance of ethanol-ethanol coupling is even greater, while at higher temperatures acetaldehyde-ethanol coupling is more likely. (iv) Although molybdenum produces acetaldehyde, it is released as a product and not C4 coupled molecules are formed from it. This is presumably because it is released from a transitional form rather than being present as adsorbed (activated) acetaldehyde.

As previously mentioned, molybdenum-containing catalysts are less basic than the WK sample. This results in the suppression of coupling reactions. In addition to the acetaldehyde formed alongside ethane, acetaldehyde that does not enter coupling reactions contributes to increased acetaldehyde selectivity. The most widely accepted theory states that the rate-determining step in ethanol coupling reactions is the dehydrogenation of ethanol to acetaldehyde. Another possible explanation for the increased amount of acetaldehyde in the product mixture

of the ethanol/acetaldehyde reaction is that when acetaldehyde is introduced into the catalytic system as a reactant, a new reaction pathway opens up. In this pathway, the formation of acetaldehyde is no longer the rate-determining step. In other words, not all of the acetaldehyde introduced as reactant or formed from ethanol reacts along the length of the catalyst bed. To gain a deeper understanding of the role of acetaldehyde fed as a reactant, further experiments and thorough kinetic modeling are needed.

5. Conclusions

In this study, wet kneaded MgO-SiO_2 with a 2/1 Mg/Si molar ratio and its 2 and 5 wt % MoO_3-containing derivatives were investigated in the reactions of ethanol and a 9/1 ethanol/acetaldehyde mixture. Structural studies have shown that as the molybdenum content increases, the isolated molybdate forms are replaced by the polymolybdate forms. The addition of molybdenum increased the acidity of the catalysts, while their basicity decreased compared to the pure MgO-SiO_2 samples. Due to the change in acid-base conditions, the selectivity of the coupled products decreased in the molybdenum-containing samples. Meanwhile, the selectivity of acetaldehyde increased and ethane appeared among the products due to the disproportionation of two adsorbed ethanol molecules on two adjacent active sites on a partially reduced molybdenum-containing catalyst. The products of the aldol condensation pathway, crotonaldehyde and crotyl alcohol, appear in the reaction of the ethanol/acetaldehyde mixture. These products can only be detected in trace amounts in the reaction of pure ethanol. Significant amounts of ethyl vinyl ether and ethyl acetate also appeared among the products at high space velocities and low temperatures. These products are formed in the condensation reactions of ethanol-acetaldehyde and acetaldehyde-acetaldehyde. Based on these results, mechanisms analogous to the formation of ethane have been proposed. These mechanisms achieve carbon-carbon coupling through the condensation of two acetaldehydes and a crotonaldehyde intermediate. It has also been suggested that introducing acetaldehyde as a reactant could create new reaction pathways. This is because ethanol dehydrogenation would no longer be the rate-determining step in the consecutive reaction chain.

CRediT authorship contribution statement

Gyula Novodárszki: Investigation. **Adél Pakuts:** Investigation. **Blanka Szabó:** Investigation, Data curation. **Hanna E. Solt:** Investigation, Data curation. **Anna Vikár:** Investigation. **Ferenc Lónyi:** Writing – review & editing, Writing – original draft, Investigation, Data curation. **Yuting Shi:** Investigation. **Amosi Makoye:** Investigation. **Róbert Barthos:** Writing – original draft, Methodology, Investigation, Data curation.

Declaration of competing interest

The authors declare that they have no known competing financial interests or personal relationships that could have appeared to influence the work reported in this paper.

Acknowledgments

One of the authors (G.N.) thanks for the support provided by the EKÖP-25 University Excellence Scholarship Program of the Ministry for Culture and Innovation from the source of the National Research, Development and Innovation Fund (ELTE Eötvös Loránd University, Budapest, Hungary).

Supplementary materials

Supplementary material associated with this article can be found, in the online version, at doi:10.1016/j.mcat.2025.115621.

Data availability

Data will be made available on request.

References

[1] E.V. Makshina, M. Dusselier, W. Janssens, J. Degrève, P.A. Jacobs, B.F. Sels, Review of old chemistry and new catalytic advances in the on-purpose synthesis of butadiene, Chem. Soc. Rev. 43 (2014) 7917–7953, https://doi.org/10.1039/C4CS00105B.
[2] K. Weissermel, H. Arpe, Industrial Organic Chemistry, Wiley, 2003, https://doi.org/10.1002/9783527619191.
[3] O.V. Larina, P.I. Kyriienko, S.O. Soloviev, Ethanol conversion to 1,3-butadiene on ZnO/MgO–SiO_2 catalysts: effect of ZnO content and MgO:siO_2 ratio, Catal. Letters. 145 (2015) 1162–1168, https://doi.org/10.1007/s10562-015-1509-4.
[4] J.L. Vieira, P. Destro, L.O. Laier, C.M.P. Marques, J.M.R. Gallo, J.M.C. Bueno, MgO/SiO_2 prepared by wet-kneading as a catalyst for ethanol conversion to 1,3-butadiene: prins condensation as the predominant mechanism, Mol. Catal. 532 (2022) 112718, https://doi.org/10.1016/j.mcat.2022.112718.
[5] W.E. Taifan, J. Baltrusaitis, Situ spectroscopic insights on the molecular structure of the MgO/SiO_2 catalytic active sites during ethanol conversion to 1,3-butadiene, J. Phys. Chem. C 122 (2018) 20894–20906, https://doi.org/10.1021/acs.jpcc.8b06767.
[6] O.V. Larina, P.I. Kyriienko, D.Y. Balakin, M. Vorokhta, I. Khalakhan, Y. M. Nychiporuk, V. Matolín, S.O. Soloviev, S.M. Orlyk, Effect of ZnO on acid-base properties and catalytic performances of ZnO/ZrO_2-SiO_2 catalysts in 1,3-butadiene production from ethanol-water mixture, Catal. Sci. Technol. 9 (2019) 3964–3978, https://doi.org/10.1039/c9cy00991d.
[7] X. Li, J. Pang, Y. Zhao, L. Li, W. Yu, F. Xu, Y. Su, X. Yang, W. Luo, M. Zheng, Identifying a bi-molecular synergetic adsorption mechanism for catalytic transformation of ethanol/acetaldehyde into 1,3-butadiene, Chinese J. Catal. 71 (2025) 297–307, https://doi.org/10.1016/S1872-2067(24)60262-7.
[8] D. Hradsky, P. Machac, D. Skoda, L. Leonova, P. Sazama, J. Pastvova, D. Kaucky, D. Vsiansky, Z. Moravec, A. Styskalik, Catalytic performance of micro-mesoporous zirconosilicates prepared by non-hydrolytic sol-gel in ethanol-acetaldehyde conversion to butadiene and related reactions, Appl. Catal. A Gen. 652 (2023) 119037, https://doi.org/10.1016/j.apcata.2023.119037.
[9] C. Angelici, F. Meirer, A.M.J. Van Der Eerden, H.L. Schaink, A. Goryachev, J. P. Hofmann, E.J.M. Hensen, B.M. Weckhuysen, P.C.A. Bruijnincx, Ex situ and operando studies on the role of copper in Cu-promoted SiO_2-MgO catalysts for the Lebedev ethanol-to-butadiene process, ACS Catal. 5 (2015) 6005–6015, https://doi.org/10.1021/acscatal.5b00755.
[10] W.E. Taifan, Y. Li, J.P. Baltrus, L. Zhang, A.I. Frenkel, J. Baltrusaitis, Operando structure determination of Cu and Zn on supported MgO/SiO_2 catalysts during ethanol conversion to 1,3-butadiene, ACS Catal. 9 (2019) 269–285, https://doi.org/10.1021/acscatal.8b03515.
[11] P.I. Kyriienko, O.V. Larina, D.Y. Balakin, M. Vorokhta, I. Khalakhan, S. A. Sergiienko, S.O. Soloviev, S.M. Orlyk, The effect of lanthanum in Cu/La(-Zr)-Si oxide catalysts for aqueous ethanol conversion into 1,3-butadiene, Mol. Catal. 518 (2022) 112096, https://doi.org/10.1016/j.mcat.2021.112096.
[12] O.V. Larina, O.V. Zikrata, L.M. Alekseenko, S.O. Soloviev, S.M. Orlyk, The effect of modification of Zn–Mg(Zr)Si oxide catalysts with rare-earth elements (Y, La, Ce) in the ethanol-to-1,3-butadiene process, Appl. Nanosci. 13 (2023) 7101–7114, https://doi.org/10.1007/s13204-023-02876-5.
[13] V.G.F. Pereira, C.R. Moreira, C.P. Rodrigues, F.S. Toniolo, Influence of active sites and the reaction conditions on the ethanol upgrading over Nb_2O_5/ZrO_2 based multifunctional catalysts, Brazilian J. Chem. Eng. 40 (2023) 1039–1054, https://doi.org/10.1007/s43153-022-00287-7.
[14] Q. Zhu, L. Yin, X. Han, B. Wang, Effect of acid–Base property on the upgrade of ethanol and acetaldehyde to butadiene over Sc_2O_3 –SiO_2 catalysts, ACS Omega. 10 (2025) 7069–7076, https://doi.org/10.1021/acsomega.4c10129.
[15] B. Szabó, G. Novodárszki, Z. May, J. Valyon, J. Hancsók, R. Barthos, Conversion of ethanol to butadiene over mesoporous In_2O_3-promoted MgO-SiO_2 catalysts, Mol. Catal. 491 (2020) 110984, https://doi.org/10.1016/j.mcat.2020.110984.
[16] J.I. Di Cosimo, V.K. Díez, M. Xu, E. Iglesia, C.R. Apesteguía, Structure and surface and catalytic properties of Mg-Al basic oxides, J. Catal. 178 (1998) 499–510, https://doi.org/10.1006/jcat.1998.2161.
[17] A.J. Scheid, E. Barbosa-Coutinho, M. Schwaab, N.P.G. Salau, Mechanism and kinetic modeling of ethanol conversion to 1-butanol over Mg and Al oxide derived from hydrotalcites, Ind. Eng. Chem. Res. 58 (2019) 12981–12995, https://doi.org/10.1021/acs.iecr.9b01491.
[18] K.V. Valihura, O.V. Larina, S.O. Soloviev, Effect of modifying additives of molybdenum and tungsten compounds on the catalytic properties of MgO-Al_2O_3 in the process of gas-phase conversion of ethanol into 1-butanol, Theor. Exp. Chem. 59 (2023) 42–50, https://doi.org/10.1007/s11237-023-09764-7.
[19] C.R. Ho, S. Shylesh, A.T. Bell, Mechanism and kinetics of ethanol coupling to butanol over hydroxyapatite, ACS Catal. 6 (2016) 939–948, https://doi.org/10.1021/acscatal.5b02672.
[20] S.C. Wang, M.C. Cendejas, I. Hermans, Insights into ethanol coupling over hydroxyapatite using modulation excitation operando infrared spectroscopy, ChemCatChem 12 (2020) 4167–4175, https://doi.org/10.1002/cctc.202000331.

[21] H. Niiyama, S. Morii, E. Echigoya, Butadiene formation from ethanol over silica-magnesia catalysts, Bull. Chem. Soc. Jpn. 45 (1972) 655–659, https://doi.org/10.1246/bcsj.45.655.
[22] W.E. Taifan, G.X. Yan, J. Baltrusaitis, Surface chemistry of MgO/SiO_2 catalyst during the ethanol catalytic conversion to 1,3-butadiene: in-situ DRIFTS and DFT study, Catal. Sci. Technol. 7 (2017) 4648–4668, https://doi.org/10.1039/c7cy01556a.
[23] G. Bozga, A.V. Brosteanu, I. Banu, A.C. Dimian, One-stage ethanol to butadiene process: analysis and design of a multi-tubular fixed bed reactor, Chem. Eng. Res. Des. 203 (2024) 608–618, https://doi.org/10.1016/j.cherd.2024.01.070.
[24] A.S. Ndou, N. Plint, N.J. Coville, Dimerisation of ethanol to butanol over solid-base catalysts, Appl. Catal. A Gen. 251 (2003) 337–345, https://doi.org/10.1016/S0926-860X(03)00363-6.
[25] E.F. de Souza, H.P. Pacheco, N. Miyake, R.J. Davis, F.S. Toniolo, Computational and experimental mechanistic insights into the ethanol-to-butanol upgrading reaction over MgO, ACS Catal 10 (2020) 15162–15177, https://doi.org/10.1021/acscatal.0c04616.
[26] A. Chieregato, J.V. Ochoa, C. Bandinelli, G. Fornasari, F. Cavani, M. Mella, On the chemistry of ethanol on basic oxides: revising mechanisms and intermediates in the Lebedev and Guerbet reactions, ChemSusChem. 8 (2015) 377–388, https://doi.org/10.1002/cssc.201402632.
[27] L. Qi, Y. Zhang, M.A. Conrad, C.K. Russell, J. Miller, A.T. Bell, Ethanol conversion to butadiene over isolated zinc and yttrium sites grafted onto dealuminated beta zeolite, J. Am. Chem. Soc. 142 (2020) 14674–14687, https://doi.org/10.1021/jacs.0c06906.
[28] J. Scalbert, F. Thibault-Starzyk, R. Jacquot, D. Morvan, F. Meunier, Ethanol condensation to butanol at high temperatures over a basic heterogeneous catalyst: how relevant is acetaldehyde self-aldolization? J. Catal. 311 (2014) 28–32, https://doi.org/10.1016/j.jcat.2013.11.004.
[29] V.L. Sushkevich, I.I. Ivanova, Mechanistic study of ethanol conversion into butadiene over silver promoted zirconia catalysts, Appl. Catal. B Environ. 215 (2017) 36–49, https://doi.org/10.1016/j.apcatb.2017.05.060.
[30] W. Tian, J.E. Herrera, Catalytic relevance of Mg-Al-O basic centers in the upgrade of ethanol to n-butanol, ChemCatChem. (2024) 202400225, https://doi.org/10.1002/cctc.202400225.
[31] T.P. Jayakumar, S.P. Suresh Babu, T.N. Nguyen, S.D. Le, R.P. Manchan, P. Phulkerd, P. Chammingkwan, T. Taniike, Exploration of ethanol-to-butadiene catalysts by high-throughput experimentation and machine learning, Appl. Catal. A Gen. 666 (2023) 119427, https://doi.org/10.1016/j.apcata.2023.119427.
[32] Y. Nakamura, T. Murayama, W. Ueda, Reduced vanadium and molybdenum oxides catalyze the equivalent formation of ethane and acetaldehyde from ethanol, ChemCatChem. 6 (2014) 741–744, https://doi.org/10.1002/cctc.201300991.
[33] C. Angelici, M.E.Z. Velthoen, B.M. Weckhuysen, P.C.A. Bruijnincx, Influence of acid-base properties on the Lebedev ethanol-to-butadiene process catalyzed by SiO_2-MgO materials, Catal. Sci. Technol. 5 (2015) 2869–2879, https://doi.org/10.1039/c5cy00200a.
[34] X. Huang, Y. Men, J. Wang, W. An, Y. Wang, Highly active and selective binary MgO-SiO_2 catalysts for the production of 1,3-butadiene from ethanol, Catal. Sci. Technol. 7 (2017) 168–180, https://doi.org/10.1039/c6cy02091g.
[35] S.-H. Chung, C. Angelici, S.O.M. Hinterding, M. Weingarth, M. Baldus, K. Houben, B.M. Weckhuysen, P.C.A. Bruijnincx, Role of magnesium silicates in wet-kneaded silica–Magnesia catalysts for the Lebedev ethanol-to-butadiene process, ACS Catal 6 (2016) 4034–4045, https://doi.org/10.1021/acscatal.5b02972.
[36] S.–H Chung, J.C.N. de Miguel, T. Li, P. Lavrik, S. Komaty, Y. Yuan, D. Poloneeva, W.H. Anbari, M.N. Hedhili, M. Zaarour, C. Martín, T. Shoinkhorova, E. Abou–Hamad, J. Gascon, J. Ruiz–Martínez, Core-shell structured magnesia-silica as a next generation catalyst for one-step ethanol-to-butadiene Lebedev process, Appl. Catal. B Environ. 344 (2024) 123628, https://doi.org/10.1016/j.apcatb.2023.123628.
[37] B. Szabó, G. Novodárszki, F. Lónyi, L. Trif, Z. Fogarassy, J. Valyon, R. Barthos, Texture and morphology-directed activity of magnesia-silica mixed oxide catalysts of ethanol-to-butadiene reaction, J. Mol. Struct. 1259 (2022) 132764, https://doi.org/10.1016/j.molstruc.2022.132764.
[38] S.-H. Chung, T. Li, T. Shoinkhorova, S. Komaty, A. Ramirez, I. Mukhambetov, E. Abou-Hamad, G. Shterk, S. Telalovic, A. Dikhtiarenko, B. Sirks, P. Lavrik, X. Tang, B.M. Weckhuysen, P.C.A. Bruijnincx, J. Gascon, J. Ruiz-Martínez, Origin of active sites on silica–magnesia catalysts and control of reactive environment in the one-step ethanol-to-butadiene process, Nat. Catal. 6 (2023) 363–376, https://doi.org/10.1038/s41929-023-00945-0.
[39] B. Szabó, G. Novodárszki, Z. Pászti, A. Domján, J. Valyon, J. Hancsók, R. Barthos, $MgO-SiO_2$ catalysts for the ethanol to butadiene reaction: the effect of Lewis acid promoters, ChemCatChem. 12 (2020) 5686–5696, https://doi.org/10.1002/cctc.202001007.
[40] B. Szabó, V. Hutkai, G. Novodárszki, F. Lónyi, Z. Pászti, Z. Fogarassy, J. Valyon, R. Barthos, A study of the conversion of ethanol to 1,3-butadiene: effects of chemical and structural heterogeneity on the activity of MgO-SiO_2 mixed oxide catalysts, React. Chem. Eng. 8 (2022) 718–731, https://doi.org/10.1039/d2re00450j.
[41] J.V. Ochoa, C. Bandinelli, O. Vozniuk, A. Chieregato, A. Malmusi, C. Recchi, F. Cavani, An analysis of the chemical, physical and reactivity features of $MgO–SiO_2$ catalysts for butadiene synthesis with the Lebedev process, Green Chem. 18 (2016) 1653–1663, https://doi.org/10.1039/C5GC02194D.
[42] E.L. Lee, I.E. Wachs, In situ spectroscopic investigation of the molecular and electronic structures of SiO 2 supported surface metal oxides, J. Phys. Chem. C. 111 (2007) 14410–14425, https://doi.org/10.1021/jp0735482.
[43] M. Thommes, K. Kaneko, A.V. Neimark, J.P. Olivier, F. Rodriguez-Reinoso, J. Rouquerol, K.S.W. Sing, Physisorption of gases, with special reference to the evaluation of surface area and pore size distribution (IUPAC Technical Report), Pure Appl. Chem. 87 (2015) 1051–1069, https://doi.org/10.1515/pac-2014-1117.
[44] P.H. Silva, D.T. Cestarolli, E.M. Guerra, Band gap values and structural changes on MoO_3 obtained by ion-exchange method, Opt. Mater. (Amst). 164 (2025) 117063, https://doi.org/10.1016/j.optmat.2025.117063.
[45] L. Li, Y. Zhao, J. Wang, R. Cui, Y. Li, L. Qi, Y. Liu, Hexagonal phase MoO_3 with three-dimensional crystal structure as heterogeneous photocatalyst for tetracycline degradation : degradation pathways and mechanism, J. Mol. Struct. 1295 (2024) 136681, https://doi.org/10.1016/j.molstruc.2023.136681.
[46] J.P. Thielemann, T. Ressler, A. Walter, G. Tzolova-Müller, C. Hess, Structure of molybdenum oxide supported on silica SBA-15 studied by Raman, UV–Vis and X-ray absorption spectroscopy, Appl. Catal. A Gen. 399 (2011) 28–34, https://doi.org/10.1016/j.apcata.2011.03.032.
[47] M. Fournier, C. Louis, M. Che, P. Chaquin, D. Masure, Polyoxometallates as models for oxide catalysts. Part I. An UV-visible reflectance study of polyoxomolybdates: influence of polyhedra arrangement on the electronic transitions and comparison with supported molybdenum catalysts, J. Catal. 119 (1989) 400–414, https://doi.org/10.1016/0021-9517(89)90170-X.
[48] R.S. Weber, Effect of local structure on the UV-visible absorption edges of molybdenum oxide clusters and supported molybdenum oxides, J. Catal. 151 (1995) 470–474, https://doi.org/10.1006/jcat.1995.1052.
[49] F.L. Martínez, M. Toledano-Luque, J.J. Gandía, J. Cárabe, W. Bohne, J. Röhrich, E. Strub, I. Mártil, Optical properties and structure of HfO_2 thin films grown by high pressure reactive sputtering, J. Phys. D. Appl. Phys. 40 (2007) 5256–5265, https://doi.org/10.1088/0022-3727/40/17/037.
[50] F. Arena, A. Parmaliana, Silica-supported molybdena catalysts: surface structures, reduction pattern, and oxygen chemisorption, J. Phys. Chem. 100 (1996) 19994–20005, https://doi.org/10.1021/jp9618587.
[51] M.L.A. Santos, H.P. Pacheco, F.S. Toniolo, Tuning acid and basic features on Mg_xAlO_y-SiO_2 impacted ethanol upgrading to 1,3-butadiene, Catal. Today. 444 (2025) 115017, https://doi.org/10.1016/j.cattod.2024.115017.